Modeling of quantum-information processing with Ehrenfest guided trajectories: A case study with spin-boson-like couplings

Sai-Yun Ye,[1] Dmitrii Shalashilin,[2] and Alessio Serafini[1]
[1]*Department of Physics and Astronomy, University College London, Gower Street, London WC1E 6BT, United Kingdom*
[2]*School of Chemistry, University of Leeds, Leeds LS2 9JT, United Kingdom*
(Received 29 January 2012; published 13 September 2012)

We apply a numerical method based on multiconfigurational Ehrenfest trajectories and demonstrate converged results for the Choi fidelity of an entangling quantum gate between two two-level systems interacting through a set of bosonic modes. We consider both spin-boson and rotating-wave Hamiltonians for various numbers of mediating modes (from 1 to 100) and extend our treatment to include finite temperatures. Our results apply to two-level impurities interacting with the same band of a photonic crystal or to two distant ions interacting with the same set of motional degrees of freedom.

DOI: 10.1103/PhysRevA.86.032312 PACS number(s): 03.67.Lx, 42.50.Ex, 42.50.Ct, 42.81.Qb

I. INTRODUCTION

The ability to track the evolution of complex quantum systems will be a crucial support to the design and development of future quantum technologies. A paradigm of particular interest for the latter is one where finite-dimensional quantum systems, typically two-level systems (qubits), interact through a "bus," made up of a set of bosonic-field modes [1–33]. In this paper, we will consider the case of two qubits interacting with a common discrete set of modes in the nonperturbative regime. Although the possibility for creating entanglement, even at steady state, by the interaction with a common bosonic bath has been highlighted repeatedly in the literature, the case of nonperturbative interactions with a bunch of 10 or 20 modes (as is the case in our paper) presents several major technical difficulties, essentially due to the impossibility of an analytic master equation approach–only possible in the continuum limit under the Born-Markov approximation—and to the huge size of the dynamically relevant part of the Hilbert space.

Various numerical approaches have been developed to emulate these dynamics on classical computers, such as the so-called multiconfigurational time-dependent Hartree method [34–36] and its "Gaussian" variation [37], various schemes based on path-integral techniques [38,39], and even the adaptation of time-adaptive density-matrix renormalization-group techniques [40] borrowed from condensed-matter theory. Here, we will tackle such difficulties by borrowing a method co-pioneered and developed by one of the authors in the arena of chemical physics [41,42]. The method is based on the adoption of a set of tensor products of time-dependent coherent states as a discrete "basis grid" on which to represent the field degrees of freedom (referred to as "coupled coherent states" in the literature [43]) and on letting the states of the comoving grid evolve according to their Ehrenfest dynamics [whose application to a grid of coherent states goes under the name of the "Multi-Configurational Eherefest" (MCE) method]. This approach has the advantage of being relatively light in terms of computational resources, easy to program, and yet allowing one to follow coherent quantum dynamics in detail, as is shown.

In our paper, we will focus on a specific, but very relevant, aspect of the quantum dynamics of the two qubits: We will consider the realization of an entangling quantum gate between them, namely, of a controlled-Z (CZ) gate. To estimate the quality of such a realization, we will consider the quantum fidelity between the pure state corresponding to the CZ gate by the standard channel-state duality (Choi isomorphism [44–46]) and the quantum state corresponding to the channel acting on the two qubits upon partial tracing over the field's degrees of freedom.

Our main aim is demonstrating the capability of Ehrenfest guided trajectories in phase space to produce reliable and converged results for complex figures of merit, able to reveal detailed information about the quantum dynamics of the constituents. The "Choi fidelity" of a two-qubit quantum gate is a property of the dynamics itself and not of the initial state, and its evaluation requires, at any time, the evolution of ten initial states: It is, therefore, a rather cumbersome figure of merit to compute, let alone to optimize over a rather large range of values of the dynamical parameters, as we did. The advantages of the Ehrenfest guided trajectories over—arguably more precise but heavier—approaches based on full variational principles are manifest in such circumstances.

As for direct impact, let us remark that our paper would apply on systems, such as two-level impurities trapped in a photonic crystal and interacting with the same band of allowed modes [32,47,48], or to the internal levels of two ions interacting with all the vibrational modes of an array of ions in a linear trap [49]. It is important to point out that our treatment can account for finite, although relatively small, temperatures as well.

Our paper is organized as follows. In Sec. II, we will review the basic theory behind methods of solution of the Schrödinger equation based on a set of time-dependent Ehrenfest guided basis states. We do not dwell so much on the technical details, which are covered elsewhere, as on the basic concepts, and try to present them in terms which are friendly to an audience with no previous familiarity with the terminology of chemical physics or molecular dynamics. In Sec. III, we will introduce the physical Hamiltonian and will precisely define our chosen figure of merit. Section IV will contain the main results of our numerical study. The entanglement generation is discussed in Sec. V. Finally, we will draw conclusions and discuss advantages and shortcomings of our method of choice in Sec. VI.

II. EHRENFEST GUIDED TRAJECTORIES

The main difficulty in dealing with a system including few two-level systems and a bunch of M bosonic modes is clearly how to handle the infinite-dimensional bosonic Hilbert space. The method we apply here, referred to in the literature as multiconfigurational Ehrenfest and first introduced in Ref. [41], tackles this difficulty on the shoulders of two major assumptions:

(i) The state space of the field modes is represented as a superposition of N time-dependent coherent states;

(ii) The time dependence of the coherent states is determined by a simplified variational principle (which, in other words, dictates how the finite-dimensional subspace spanned by the set of coherent states changes with time, trying to keep it in the dynamically relevant region).

The finite-dimensional systems involved are, on the other hand, treated by representing their entire Hilbert space, spanned by d orthonormal basis states $|l\rangle$, for $l \in \{1,\ldots,d\}$. In agreement with (i), the ansatz wave function of the whole system reads

$$|\psi\rangle = \sum_{l=1}^{d}\sum_{j=1}^{N} c_{l,j}(t)[|l\rangle \otimes |\boldsymbol{\alpha}_j(t)\rangle], \tag{1}$$

where $\boldsymbol{\alpha}_j \in \mathbb{C}^M \ \forall\, j$ and each $|\boldsymbol{\alpha}_j\rangle$ is a tensor product of coherent states: $|\boldsymbol{\alpha}_j\rangle = \bigotimes_{m=1}^{M} |\alpha_j^{(m)}\rangle$ such that, if a_m is the annihilation operator of mode m, one has $a_m|\boldsymbol{\alpha}_j\rangle = \alpha_j^{(m)}|\boldsymbol{\alpha}_j\rangle$. Since we will be dealing with two qubits, it will be $d = 4$ for us.

The evolution of the dynamical parameters is more conveniently described by adopting a Lagrangian formulation. For a Hamiltonian operator $\hat{H}$, let us define $\mathcal{L}$ as

$$\mathcal{L} = \langle\psi|\hat{H} - i\,\partial_t|\psi\rangle. \tag{2}$$

The time-derivative operator is defined as the differentiation of the time-dependent coefficients $c_{l,j}$ and by the relationships $\partial_t|l\rangle = 0$ (the finite-dimensional system's basis is time independent) and $\partial_t|\boldsymbol{\alpha}_j\rangle = \sum_{m=1}^{M}[\dot{\alpha}_j^{(m)}(a_m^\dagger - \alpha_j^{(m)*}/2) - \dot{\alpha}_j^{(m)*}\alpha_j^{(m)}/2]|\boldsymbol{\alpha}_j\rangle$ (derived from the time dependence of a coherent state with varying phase-space position). The quantity $\mathcal{L}$ is, hence, a function of the coefficients $c_{l,j}$, the complex parameters $\boldsymbol{\alpha}_j$, and their time derivatives $\dot{c}_{l,j}$ and $\dot{\boldsymbol{\alpha}}_j$. In fact, it can be shown that $\mathcal{L}$ serves as a Lagrangian for the quantum system in the sense that the Euler-Lagrange equations,

$$\frac{\partial\mathcal{L}}{\partial c_{l,j}} = \frac{d}{dt}\frac{\partial\mathcal{L}}{\partial\dot{c}_{l,j}} \tag{3}$$

are *equivalent* to the Schrödinger equation.[1] See Appendix B for more details.

Besides determining the state evolution, the variational formalism also provides one with a recipe to update the basis such that the expression $\mathcal{L}$ in Eq. (2), which clearly always equals 0 in the exact dynamics, is minimized during the time evolution. Such a minimization, which, in essence, keeps the basis in the "most relevant" region of the Hilbert space within the constraints of the adopted approximation, would be obtained by considering the full Euler-Lagrange equations for the $M \times N$ complex parameters $\boldsymbol{\alpha}_j$ and their time derivatives. This would be a large nonlinear system of coupled equations, requiring a substantial numerical effort to be solved. Instead, we introduce, here, assumption (ii) and replace the full variational equations for $\boldsymbol{\alpha}_j$ with a simplified version thereof. In particular, we will neglect all terms coupling the different $\boldsymbol{\alpha}_j$'s on the grounds that the overlaps $\langle\boldsymbol{\alpha}_j|\boldsymbol{\alpha}_k\rangle$ are typically very small if the number of modes M is large enough. For each j, let us then define the vector $|\tilde{\psi}_j\rangle$ as

$$|\tilde{\psi}_j\rangle = \sum_{l=1}^{d} c_{l,j}|l\rangle \otimes |\boldsymbol{\alpha}_j\rangle, \tag{4}$$

and the corresponding "approximated" Lagrangian $\tilde{\mathcal{L}}_j$ as

$$\tilde{\mathcal{L}}_j = \langle\tilde{\psi}_j|H - i\,\partial_t|\tilde{\psi}_j\rangle. \tag{5}$$

The equation of motion for the parameter $\alpha_j^{(m)}$ (the mth component of the vector $\boldsymbol{\alpha}_j$) is

$$\frac{\partial\tilde{\mathcal{L}}_j}{\partial\alpha_j^{(m)}} = \frac{d}{dt}\frac{\partial\tilde{\mathcal{L}}_j}{\partial\dot{\alpha}_j^{(m)}}, \tag{6}$$

where we also neglect the time dependence of the coefficients $c_{l,j}$ such that each Lagrangian $\tilde{\mathcal{L}}_j$ only depends on the four complex parameters $c_{l,j}$ and on the M complex parameters represented by the entries of $\boldsymbol{\alpha}_j$ (and on their time derivatives $\dot{\boldsymbol{\alpha}}_j$, see Appendix A for further details). Equation (6) defines the MCE method we are using.

Notice that the assumption (ii) is not, per se, an approximation, but rather just a way of choosing the time dependence of the adopted basis. However, it should be stressed that, in general, the exact Euler-Lagrange equation for the full variation in the parameters $\alpha_j^{(m)}$ is likely to provide one with a more accurate result in that it yields a smaller Lagrangian $|\mathcal{L}|$ (which is zero in the exact dynamics).

However, Eq. (6) is much easier to treat numerically, hence, the advantage of our method, which can be easily programed and applied with modest computational resources and often provides results in very good agreement with complete variational methods, such as Multi-Configuration Time-Dependent Hartree (MCTDH) or Gaussian-based MCTDH (G-MCTDH) [34–37].

Multiconfigurational Ehrenfest guided trajectories have been thoroughly tested for spin-boson dynamics under different spectral densities, establishing the reliability of their converged results in several diverse situations [41,50]. Here, we will instead apply them to study a composite system including discrete sets of bosonic-field modes where coherent quantum-information processing can be carried out.

III. MODEL AND FIGURE OF MERIT

We set out to study coherent quantum-information processing for a system comprising two two-level systems (qubits)

[1] To be precise, in our instance, since the infinite-dimensional Hilbert space is only approximately represented by a basis of $4N$ vectors, such equations are equivalent to the projection of the Schrödinger equation on the subspace spanned by our basis.

connected by M bosonic modes through a spin-boson-like coupling.

In principle, this represents the archetype of a quantum system where complex dynamics and information-processing tasks can be carried out, and whose dynamics is impervious to nonapproximated methods. In practice, our case study may be thought of as representing two two-level atoms (or impurities) interacting with the same photonic band of a photonic crystal [47] or a simulation of the same setting in a linear array of trapped ions (where the qubits are embodied by internal levels of the ions interacting with the same set of vibrational normal modes [49]).

For future convenience, let us relabel the four states of the computational basis of the two two-level systems as follows:

$$|1\rangle = |\downarrow\downarrow\rangle, \tag{7}$$

$$|2\rangle = |\downarrow\uparrow\rangle, \tag{8}$$

$$|3\rangle = |\uparrow\downarrow\rangle, \tag{9}$$

$$|4\rangle = |\uparrow\uparrow\rangle. \tag{10}$$

The operators $\hat{\sigma}_x^{(1)}$, $\hat{\sigma}_x^{(2)}$, $\hat{\sigma}_z^{(1)}$, and $\hat{\sigma}_z^{(2)}$, will stand for the customary Pauli operators in the Hilbert spaces of qubits 1 and 2. For instance, in the adopted basis, $\hat{\sigma}_x^{(1)}$ is defined by $\hat{\sigma}_x^{(1)}|1\rangle = |3\rangle$, $\hat{\sigma}_x^{(1)}|3\rangle = |1\rangle$, $\hat{\sigma}_x^{(1)}|2\rangle = |4\rangle$, and $\hat{\sigma}_x^{(1)}|4\rangle = |2\rangle$.

In our paper, we will consider both an actual spin-boson-like Hamiltonian,

$$\hat{H} = \sum_{j=1}^{2}\left(\frac{\varepsilon}{2}\hat{\sigma}_z^{(j)} + \frac{\Delta_j}{2}\hat{\sigma}_x^{(j)}\right) + \sum_{m=1}^{M}\omega_m a_m^\dagger a_m + \sum_{j=1}^{2}\sum_{m=1}^{M}\left[g_m^{(j)}\sigma_x^{(j)}(a_m + a_m^\dagger)\right], \tag{11}$$

and its rotating-wave counterpart:

$$\hat{H}_{\rm rw} = \sum_{j=1}^{2}\left(\frac{\varepsilon}{2}\hat{\sigma}_z^{(j)} + \frac{\Delta_j}{2}\hat{\sigma}_x^{(j)}\right) + \sum_{m=1}^{M}\omega_m a_m^\dagger a_m + \sum_{j=1}^{2}\sum_{m=1}^{M}\left[g_m^{(j)}(\sigma_+^{(j)}a_m + \sigma_-^{(j)}a_m^\dagger)\right], \tag{12}$$

where $\sigma_+^{(j)} = \sigma_-^{(j)\dagger} = \sigma_x^{(j)} + i\sigma_y^{(j)}$. As is well known, the Hamiltonian $\hat{H}_{\rm rw}$ is a good approximation of $\hat{H}$ with $\Delta_j = 0$ for $j = 1,2$ in the almost resonant high-frequency case, that is, in our notation, for $|2\varepsilon - \omega_m| \ll |2\varepsilon + \omega_m|$, $\forall\, m$. In the following, we will consider systems with different numbers of bosonic modes M, various values of frequencies $\{\omega_m\}$ and spin-boson couplings $\{g_m^{(j)}\}$, and different values of the tunneling parameters Δ_j. Also, we will set $\hbar = 1$ throughout the paper.

In reproducing the dynamics of the two qubits by treating the field through multiconfigurational Ehrenfest trajectories, we will aim at obtaining converged results for a figure of merit of interest in the study of quantum-information processing, namely, the fidelity with which an entangling CZ gate can be realized for the two qubits through the mediating bosonic modes. In terms of the basis states of Eqs. (7)–(10), a CZ gate is represented as a unitary $U_{\rm cz}$ leaving all the basis states invariant except for $|4\rangle$, which becomes $-|4\rangle$, that is

$$U_{\rm cz}|j\rangle = f(j)|j\rangle \quad \text{for} \quad 1 \leqslant j \leqslant 4, \tag{13}$$

where $f(j) = 1$ for $j \in \{1,2,3\}$ and $f(j) = -1$ for $j = 4$. The relevance of a CZ gate to quantum-information processing stems from its being a maximally entangling gate which, combined with single-qubit unitaries, forms a universal quantum set for gate-based quantum computation [51].

At zero temperature, the quantum operation Γ_t we want to compare with the CZ unitary gate is defined as follows in terms of a notional initial density matrix of the qubits ϱ:

$$\Gamma_t(\varrho) = {\rm Tr}_B[e^{-i\hat{H}t}(\varrho \otimes |0\rangle\langle 0|)e^{i\hat{H}t}], \tag{14}$$

where ${\rm Tr}_B$ stands for partial tracing over the Hilbert space of the bosonic modes and $|0\rangle$ is the vacuum state of the modes. We will also extend our treatment to include a finite temperature $1/\beta$ of the bosonic modes (in natural units where $k_B = 1$), in which case, the quantum operation $\Gamma_{t,\beta}$ will be given by

$$\Gamma_{t,\beta}(\varrho) = {\rm Tr}_B\left[e^{-i\hat{H}t}\left(\varrho \otimes \int_{\mathbb{C}^{2M}} P_\beta(\boldsymbol{\alpha})|\boldsymbol{\alpha}\rangle\langle\boldsymbol{\alpha}|d^{2M}\boldsymbol{\alpha}\right)e^{i\hat{H}t}\right], \tag{15}$$

with

$$P_\beta(\boldsymbol{\alpha}) = \prod_{m=1}^{M}\left(\frac{e^{\beta\omega_m} - 1}{\pi}e^{-(e^{\beta\omega_m}-1)|\alpha_m|^2}\right). \tag{16}$$

The function $P_\beta(\boldsymbol{\alpha})$ is just the Glauber-Sudarshan P representation of a thermal state of the bosonic modes (given by the product of individual P representations for each of the modes). In our notation, $\boldsymbol{\alpha} \in \mathbb{C}^{2M}$, whereas, each component of $\boldsymbol{\alpha}$ is denoted by α_m. Clearly, one has that $\lim_{\beta\to\infty}\Gamma_{t,\beta} = \Gamma_t$.

In our numerical paper, we reproduce the operations Γ_t by adopting the method detailed in the previous section, which is defined for pure states, and reconstruct the operations $\Gamma_{t,\beta}$ by sampling different initial pure coherent states $|\boldsymbol{\alpha}\rangle$ for the field according to the distribution given by $P(\boldsymbol{\alpha})$. We will describe the field in terms of coupled coherent states during the time evolution and then will trace it out to achieve the quantum operation acting on the two qubits.

To define the gate fidelity F, we will make use of the classic channel-state duality (Choi isomorphism) mapping linear quantum operations over a Hilbert space $\mathcal{H}$ into quantum states on the Hilbert space $\mathcal{H}\otimes\mathcal{H}$ [45]. Turning to the two-qubit Hilbert space $\mathcal{H}$ spanned by the basis states (7)–(10), let us define the maximally entangled fiducial state $|\psi\rangle$ (belonging to $\mathcal{H}^2$) as

$$|\psi\rangle = \tfrac{1}{2}(|1\rangle\otimes|1\rangle + |2\rangle\otimes|2\rangle + |3\rangle\otimes|3\rangle + |4\rangle\otimes|4\rangle). \tag{17}$$

For a generic CP map Ω, the corresponding quantum state ϱ_Ω may be defined as

$$\varrho_\Omega = (\Omega\otimes\mathbb{1})(|\psi\rangle\langle\psi|), \tag{18}$$

where $\mathbb{1}$ is the identity map acting on $\mathcal{H}$.

Since the CZ gate is unitary, the quantum state $\varrho_{\rm cz}$ is bound to be pure: $\varrho_{\rm cz} = |\varphi_{\rm cz}\rangle\langle\varphi_{\rm cz}|$ with

$$|\varphi_{\rm cz}\rangle = \frac{1}{2}(|1\rangle\otimes|1\rangle + |2\rangle\otimes|2\rangle + |3\rangle\otimes|3\rangle - |4\rangle\otimes|4\rangle) = \frac{1}{2}\sum_{j=1}^{4} f(j)(|j\rangle\otimes|j\rangle). \quad (19)$$

The state $\varrho_{\Gamma_{t,\beta}}$ corresponding to $\Gamma_{t,\beta}$ is, instead, given by

$$\varrho_{\Gamma_{t,\beta}} = \frac{1}{4}\sum_{j,k=1}^{4}\Gamma_{t,\beta}(|j\rangle\langle k|)\otimes|j\rangle\langle k|. \quad (20)$$

We can then naturally define the CZ operation fidelity F (which we will informally refer to as the Choi fidelity) as the overlap,

$$F = \langle\varphi_{\rm cz}|\varrho_{\Gamma_{t,\beta}}|\varphi_{\rm cz}\rangle = \sum_{j,k=1}^{4}\frac{f(j)f(k)}{16}\langle j|\Gamma_{t,\beta}(|j\rangle\langle k|)|k\rangle. \quad (21)$$

The quantity F captures, in one real number, a relevant facet of the quantum dynamics governing the two qubits. Its relationship to quantum coherence is manifest in that, if the off-diagonal elements between the basis vectors of Eqs. (7)–(10) are set to zero, then one has $F \leqslant 1/4$. Any value of F larger than $1/4$ is, thus, in a sense, a signature of quantum coherence. More importantly, F is also a measure of how well a coherent quantum task can be performed and is strictly related to the entanglement generated between the two qubits (in that entanglement, a perfect CZ gate would get entanglement equal to 1 ebit for a properly chosen initial state). Moreover, F, although partial to the chosen reference gate (CZ in this case), is completely independent of the initial state and represents a property of the *dynamics* alone.

Of course, we could have chosen more generic quantifiers, such as, for instance, the largest eigenvalue of the operator $\varrho_{\Gamma_{t,\beta}}$, which would equal 1 in the ideal case where the qubits undergo a unitary evolution and would quantify, in a sense, the overall coherence of the qubits' evolution. However, we deem such choices to be less informative with regard to the applicative potential of a complex dynamics.

Given a potentially useful quantum dynamics, the knowledge of F is instead very desirable to possess. Demonstrating the use of a numerical technique capable of providing one with reliable estimates of F in relevant situations is, in a nutshell, the aim of the current analysis.

IV. CHOI FIDELITY OF THE CZ GATE

Here, we will slightly deviate from the previously adopted notation by setting $g_l^{(j)} = g_j$ for all j and l. It is important to remark that assuming equal couplings between each qubit and all the modes is in no way essential to our numerical approach. Such an assumption can be—and will be, in the following—relaxed if need be.

Let us then, to begin with, set the coupling between the first qubit and the field modes g_1 to 1 and essentially choose it as the unit of time. Let us also, until further notice, set $\varepsilon = \Delta = 0$, $\beta \to \infty$ (zero temperature) and consider the rotating-wave Hamiltonian $\hat{H}_{\rm rw}$. Note that the Hamiltonian $\hat{H}_{\rm rw}$ with

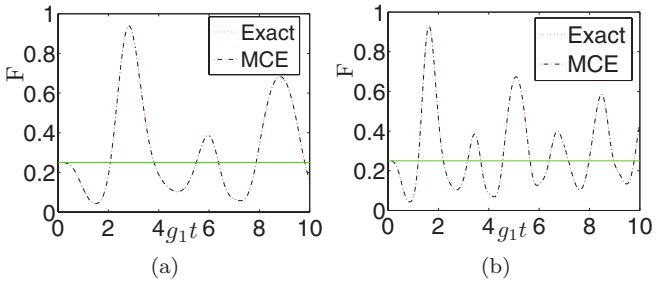

FIG. 1. (Color online) Choi fidelity F versus rescaled time for $\hat{H}_{\rm rw}$ with $\varepsilon = \Delta = 0$, $g_1 = 1$, and $g_2 = 1.9$, obtained at zero temperature by the dot-dashed curve: MCE method and dotted curve: exact analytic integration for (a) $M = 1$ and $\omega_1 = 0.1$ and (b) $M = 3$ and $\omega_m = 0.1m$ for $1 \leqslant m \leqslant 3$. The lines $F = 0.25$ are reported for reference. All the quantities plotted are dimensionless.

$\varepsilon = \Delta = 0$ can be derived from the full Hamiltonian $\hat{H}$ with $\Delta = 0$ by switching to the interaction picture and applying the rotating-wave approximation: Thus, ε can be set to zero, and each field frequency ω_m is shifted as per $\omega_m \to \omega_m - 2\varepsilon$.

By exploiting the conservation of the number of excitations, the dynamics governed by the Hamiltonian $\hat{H}_{\rm rw}$ for $\Delta = 0$ can easily be solved analytically. The agreement between such analytical solutions and the MCE results has been tested for up to ten modes and is excellent. Figures 1(a) and 1(b) show such an agreement in terms of CZ Choi fidelity F for $g_2 = 1.9$ and one mode with $\omega_1 = 0.1$ and three modes with $\omega_1 = 0.1$, $\omega_2 = 0.2$, and $\omega_3 = 0.3$, respectively. An initial peak with fidelity larger than 0.9 is immediately apparent: This peak is the main object of our investigation for larger numbers of modes too. For three modes, the peak appears at a time, which is approximately reduced by a $\sqrt{3}$ factor with respect to the single-mode case. This cooperative effect is confirmed for all numbers of modes up to 20 and is simply due to the fact that the qubits are coupled to the field through the mode $\frac{1}{\sqrt{M}}\sum_{m=1}^{M} a_m$ with an effective coupling, which scales like $\sqrt{M}$ (clearly, this is the consequence of assuming equal couplings with all modes).

Figures 2–6 depict a detailed analysis of the Choi fidelity for $M = 10$ bosonic modes with frequencies $\omega_m = 0.1m$ for

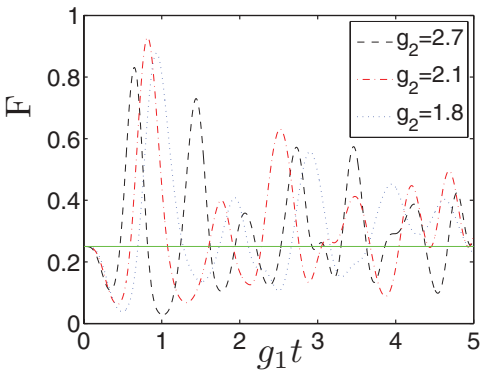

FIG. 2. (Color online) MCE results for the Choi fidelity F versus rescaled time for $\hat{H}_{\rm rw}$ with $\varepsilon = \Delta = 0$, $g_1 = 1$, $M = 10$, and $\omega_m = 0.1m$ for $1 \leqslant m \leqslant 10$, zero temperature, and different values of g_2. The line $F = 0.25$ is reported for reference. All the quantities plotted are dimensionless.

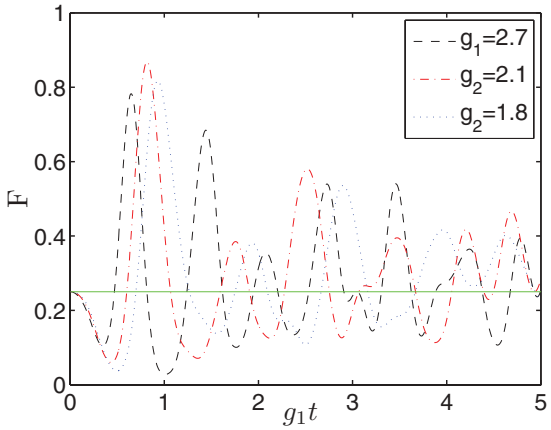

FIG. 3. (Color online) MCE results for the Choi fidelity F versus rescaled time for $\hat{H}_{\rm rw}$ with $\varepsilon = \Delta = 0$, $g_1 = 1$, $M = 10$, and $\omega_m = 0.1m$ for $1 \leqslant m \leqslant 10$, $\beta = 10$, and different values of g_2. The line $F = 0.25$ is reported for reference. All the quantities plotted are dimensionless.

$1 \leqslant m \leqslant 10$, three different temperatures ($\beta \to \infty$, $\beta = 10$, and $\beta = 5$), and different values of the coupling g_2, scanned over the range of 1.8–2.7. The zero-temperature case (Fig. 2) shows how the dispersion of quantum coherence among the field's degrees of freedom affects the gate's fidelity (whose maximum is smaller than in the one- and three-mode cases), although in the considered region of dynamical parameters, the effect is not as pronounced as one could imagine. The plots clearly show the detrimental effect of thermal fluctuations on coherent quantum effects, even at such relatively low temperatures. In practice, this analysis suggests severe constraints on the temperature for the observation of coherent quantum effects mediated by discrete vibrational modes (typically, much more susceptible to thermal excitations than optical modes due to their lower frequencies), considering that the highest temperature accounted for is around $0.2g_1$ in natural units: Even in the rather optimistic hypothesis of couplings on the order of 1 GHz, the temperature needed to observe coherent oscillations is on the order of a millikelvin, and this estimate decreases linearly with the coupling.

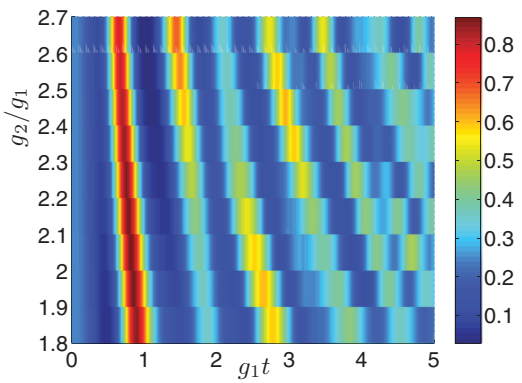

FIG. 4. (Color online) MCE results for the Choi fidelity F versus rescaled time for $\hat{H}_{\rm rw}$ with $\varepsilon = \Delta = 0$, $g_1 = 1$, $M = 10$, and $\omega_m = 0.1m$ for $1 \leqslant m \leqslant 10$, $\beta = 10$, and different values of g_2/g_1 (red stands for higher values, and blue stands for lower values). All the quantities plotted are dimensionless.

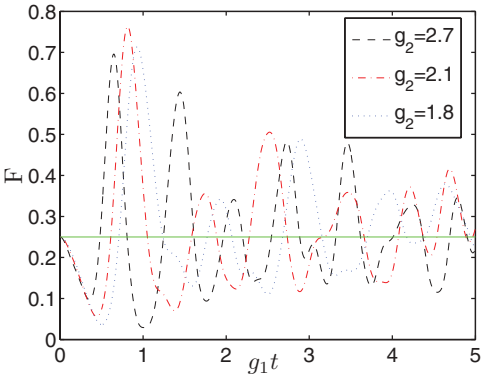

FIG. 5. (Color online) MCE results for the Choi fidelity F versus rescaled time for $\hat{H}_{\rm rw}$ with $\varepsilon = \Delta = 0$, $g_1 = 1$, $M = 10$, and $\omega_m = 0.1m$ for $1 \leqslant m \leqslant 10$, $\beta = 5$, and different values of g_2/g_1. The line $F = 0.25$ is reported for reference. All the quantities plotted are dimensionless.

Most importantly, we were able to determine the optimal value of the coupling g_2 with respect to a vast range of values (much wider than what was reported in the plots) in terms of the maximal converged Choi fidelity F and to establish that $g_2 \simeq 2.1$ yields the closest results to an ideal CZ gate. Clearly, in practice, such couplings will not always be tunable at will, or possibly only within a given window of values. Anyway, it is very remarkable to be able to identify optimal values of the dynamical parameters given a specific sophisticated dynamical figure of merit. Notice that, due to the complexity of the figure of merit adopted, this kind of optimization would be next to impossible to perform analytically, even for most solvable systems. This case, hence, demonstrates particularly well the potential of our tools.

Let us now turn to a case, which cannot be treated analytically by switching on the local tunneling rate Δ. In particular, let us consider $\varepsilon = \Delta = 1$ and $\omega_m = 0.1m$ for $1 \leqslant m \leqslant 10$. As usual, we set $g_1 = 1$ and consider different values of g_2 and different temperatures (zero temperature and $\beta = 10$): The values of F for such a configuration are displayed in Figs. 7–10. The initial peak in F is still apparent,

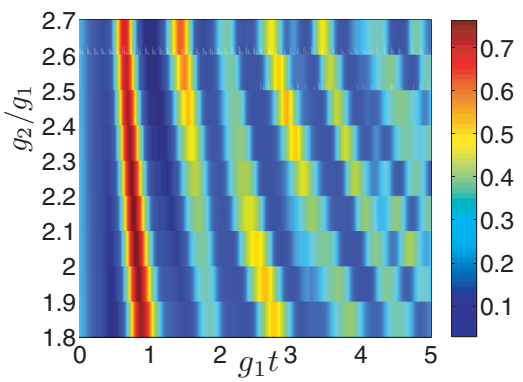

FIG. 6. (Color online) MCE results for the Choi fidelity F versus rescaled time for $\hat{H}_{\rm rw}$ with $\varepsilon = \Delta = 0$, $g_1 = 1$, $M = 10$, and $\omega_m = 0.1m$ for $1 \leqslant m \leqslant 10$, $\beta = 5$, and different values of g_2/g_1 (red stands for higher values, and blue stands for lower values). All the quantities plotted are dimensionless.

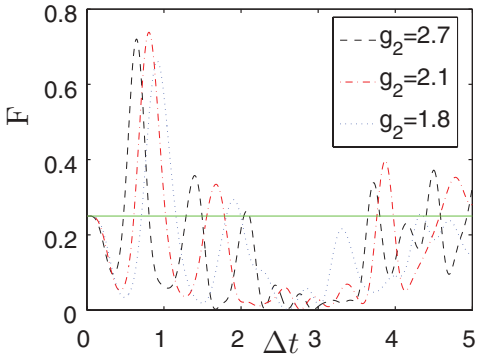

FIG. 7. (Color online) MCE results for the Choi fidelity F versus rescaled time at zero temperature for $\hat{H}_{\rm rw}$ with $\varepsilon = \Delta = 1$, $g_1 = 1$, $M = 10$, and $\omega_m = 0.1m$ for $1 \leqslant m \leqslant 10$ and different values of g_2. The line $F = 0.25$ is reported for reference. All the quantities plotted are dimensionless.

but the breaking of the phase invariance by the term Δ clearly degrades the quality of the gate with a maximum Choi fidelity, which is now around 0.7, even at zero temperature. This poorer performance is understandable in that the tunneling terms add an intrinsic rotation to the local bases of the two qubits, whose mismatch with the oscillations mediated by the bosonic modes is responsible for the decay in the quality of the CZ gate.

We now turn to the full spin-boson-like Hamiltonian $\hat{H}$ (including the counter-rotating terms in the qubit-field coupling) and consider the cases $\varepsilon = \Delta = 1$ and $\omega_m = 0.1m$ for $1 \leqslant m \leqslant 10$. The inclusion of the counter-rotating terms makes the simulation much more challenging to run and to converge. Roughly speaking, the main difficulty one encounters comes down to the fact that the time derivatives of the phase-space positions of the basis grid, determined by the Ehrenfest dynamics as per Eq. (6), are much larger if the counter-rotating terms are included. The time-dependent grid, thus, evolves much more rapidly in phase space and is likely to leave the dynamically relevant region and to accumulate substantial errors earlier. We were, however, able to obtain well-converged results by reducing the coupling g_1 to 0.5, which is still very far from the perturbative regime (see

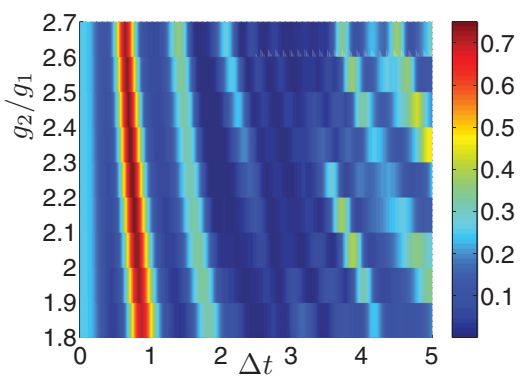

FIG. 8. (Color online) MCE results for the Choi fidelity F versus rescaled time at zero temperature for $\hat{H}_{\rm rw}$ with $\varepsilon = \Delta = 1$, $g_1 = 1$, $M = 10$, and $\omega_m = 0.1m$ for $1 \leqslant m \leqslant 10$ and different values of g_2/g_1 (red stands for higher values, and blue stands for lower values). All the quantities plotted are dimensionless.

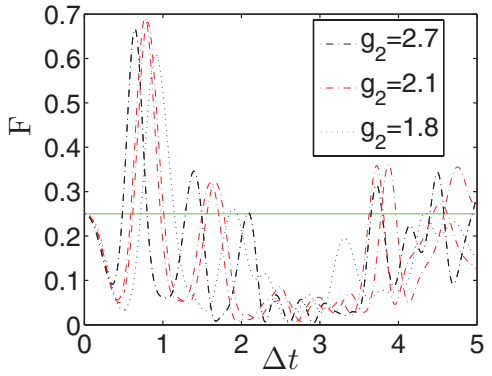

FIG. 9. (Color online) MCE results for the Choi fidelity F versus rescaled time for $\hat{H}_{\rm rw}$ with $\varepsilon = \Delta = 1$, $g_1 = 1$, $M = 10$, and $\omega_m = 0.1m$ for $1 \leqslant m \leqslant 10$, $\beta = 10$, and different values of g_2. The line $F = 0.25$ is reported for reference. All the quantities plotted are dimensionless.

Appendix C for a more detailed discussion concerning the convergence of our numerics). Likewise, we scanned values of g_2 up to 0.5. Quite significantly—as confirmed by Figs. 11 and 12, respectively, for zero temperature and $\beta = 10$—we could not find any value of g_2 such that the Choi fidelity of the CZ gate reached 0.25. In fact, strong enough couplings are necessary to entangle the two qubits on short enough time scales but, with such strong couplings, the counter-rotating terms heat the qubits up too quickly for coherent effects to take place, at least, in this region of parameters. This heating overshadows the effect of thermal fluctuations in the field, which are barely noticeable for $\beta = 10$ (and are, instead, manifest in the rotating-wave regime at the same temperature).

In order to simulate the effect of a band of a one-dimensional photonic band-gap medium where modes are usually doubly degenerate in frequency (since they can propagate in either spatial direction), we have also considered a case with $M = 20$ modes, two for each equally spaced frequency. All the other parameters have been kept as above with $\varepsilon = \Delta = 1$ and $g_1 = 1$ in the rotating-wave case (Fig. 13), and $g_1 = 0.5$ in the full Hamiltonian (Fig. 14). Comparing Fig. 13 with Fig. 7 shows

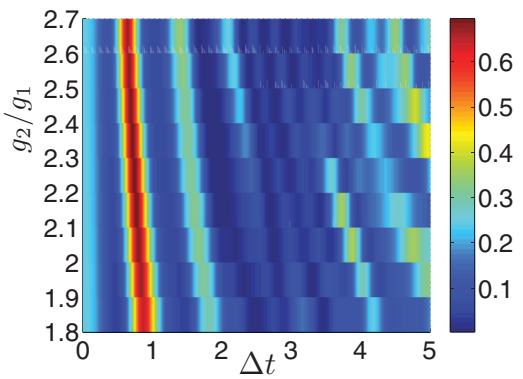

FIG. 10. (Color online) MCE results for the Choi fidelity F versus rescaled time for $\hat{H}_{\rm rw}$ with $\varepsilon = \Delta = 1$, $g_1 = 1$, $M = 10$, and $\omega_m = 0.1m$ for $1 \leqslant m \leqslant 10$, $\beta = 10$, and different values of g_2/g_1 (red stands for higher values, and blue stands for lower values). All the quantities plotted are dimensionless.

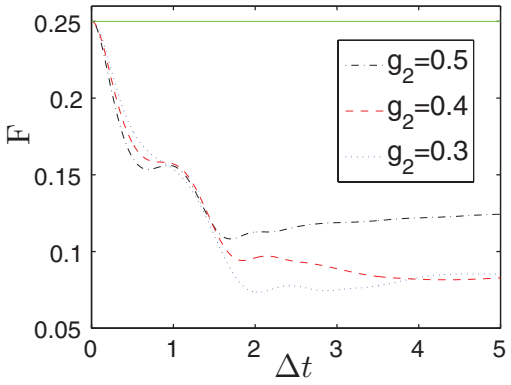

FIG. 11. (Color online) MCE results for the Choi fidelity F versus rescaled time at zero temperature for $\hat{H}$ with $\varepsilon = \Delta = 1$, $g_1 = 0.5$, $M = 10$, and $\omega_m = 0.1m$ for $1 \leqslant m \leqslant 10$ and different values of g_2. The line $F = 0.25$ is reported for reference. All the quantities plotted are dimensionless.

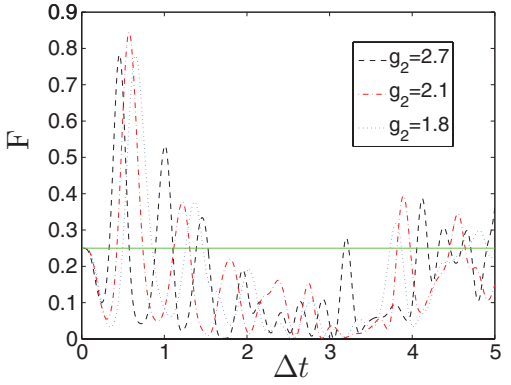

FIG. 13. (Color online) MCE results for the Choi fidelity F versus rescaled time at zero temperature for $\hat{H}_{\rm rw}$ with $\varepsilon = \Delta = 1$, $g_1 = 1$, $M = 20$, and $\omega_m = 0.1m$ for $1 \leqslant m \leqslant 10$, $\omega_m = 0.1(m-10)$ for $11 \leqslant m \leqslant 20$ and different values of g_2. The line $F = 0.25$ is reported for reference. All the quantities plotted are dimensionless.

that the initial peak in Choi fidelity is still present: Moreover, not only does it occur earlier by a factor $\sqrt{2}$ (as expected because of the cooperation between the modes due to the balanced coupling), but also it is higher. Contrary to common intuition, this example shows that a larger number of mediating modes, in favorable dynamical configurations, such as this, can actually be advantageous for the implementation of distributed coherent dynamics. Note that, for $M = 20$ modes, we needed about $N = 400$ coupled coherent states to achieve converged results. This is as large a basis set as we used in this paper.

A. Zero-temperature Ohmic spin-boson bath

The notion of entangling separated systems and of distributing quantum coherence by interaction with common heat baths or other incoherent means is well established in the quantum-information and condensed-matter communities and has been explored under a number of—either more specific and applied or more general and abstract—viewpoints [52–66]. However, the problem of studying the nonperturbative interaction of two qubits with a common bath is still, in general, a difficult one. Thus, to provide the reader with further evidence of the versatility and power of our approach, we also report the application of the MCE method to the controlled-Z Choi fidelity for the case of the spin-boson Hamiltonian $\hat{H}$ with $\varepsilon = \Delta = 1$ and both qubits interacting with a common bath at zero temperature and with Ohmic spectral density $J(\omega)$ given by

$$J(\omega) = \frac{2}{\pi}\alpha\omega e^{-\omega/\omega_c}, \tag{22}$$

where α is the Kondo parameter, which we fix at 0.09 and ω_c is a cutoff frequency.

We use a standard approach to discretize the bath, which has already been proven to be very reliable for single-spin Ohmic spin-boson systems [41]. In particular, the frequencies and coupling strengths are chosen as follows:

$$\omega_m = -\omega_c \ln\left[1 - \frac{m(1 - e^{-\omega_{\max}/\omega_c})}{M}\right], \tag{23}$$

$$g_m^1 = g_m^2 = \sqrt{\frac{\omega_m \alpha \omega_c (1 - e^{-\omega_{\max}/\omega_c})}{2M}}, \tag{24}$$

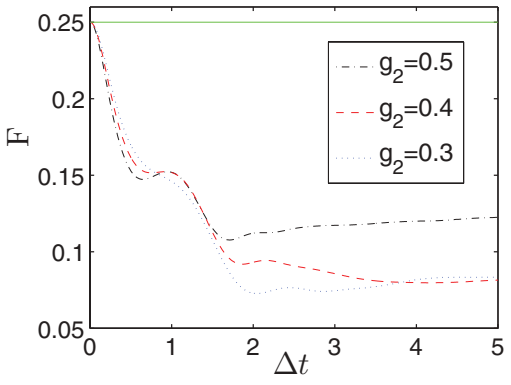

FIG. 12. (Color online) MCE results for the Choi fidelity F versus rescaled time for $\hat{H}$ with $\varepsilon = \Delta = 1$, $g_1 = 0.5$, $M = 10$, and $\omega_m = 0.1m$ for $1 \leqslant m \leqslant 10$, $\beta = 10$, and different values of g_2. The line $F = 0.25$ is reported for reference. All the quantities plotted are dimensionless.

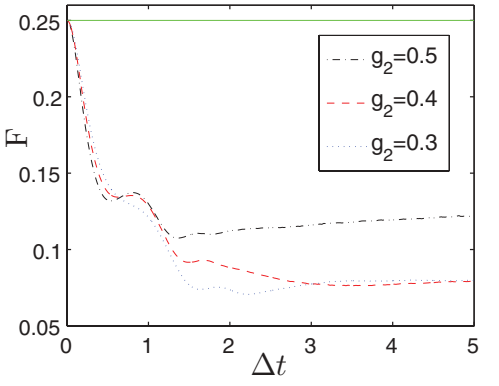

FIG. 14. (Color online) MCE results for the Choi fidelity F versus rescaled time at zero temperature for $\hat{H}$ with $\varepsilon = \Delta = 1$, $g_1 = 0.5$, $M = 20$, and $\omega_m = 0.1m$ for $1 \leqslant m \leqslant 10$, $\omega_m = 0.1(m-10)$ for $11 \leqslant m \leqslant 20$ and different values of g_2. The line $F = 0.25$ is reported for reference. All the quantities plotted are dimensionless.

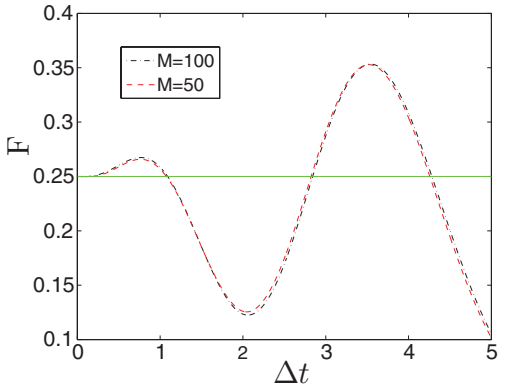

FIG. 15. (Color online) MCE results for the Choi fidelity F versus rescaled time at zero temperature for $\hat{H}$ with $\varepsilon = \Delta = 1$ and a common Ohmic bath with $\alpha = 0.09$, $\omega_c = 2.5$, and different numbers of total bath modes. The line $F = 0.25$ is reported for reference. All the quantities plotted are dimensionless.

where $\omega_{\max}$ is a free parameter of the numerics, which we converge our results against (in that we choose it large enough to obtain converged results). In particular, we choose $\omega_{\max} = 12.5$ for $\omega_c = 2.5$ and $\omega_{\max} = 6$ for $\omega_c = 1$. Also, the coupling strengths g_m^j are defined as in Eqs. (11) and (12).

Figure 15 shows the convergence of our results for $\omega_c = 2.5$ and the full Hamiltonian $\hat{H}$ in terms of the total number of modes in the bath ($M = 50$ and $M = 100$). It is apparent that, in this instance, a gate fidelity higher than the threshold value 0.25—implying the presence of coherent off-diagonal terms in the computational basis of the two qubits—can actually be achieved even for the full spin-boson Hamiltonian. So, quite interestingly, if the counter-rotating terms are included, one obtains larger gate fidelities when mimicking a bath than for a smaller set of discrete bus frequencies. Of-resonant modes are more influential in the full Hamiltonian, and their impact seems to be captured faithfully by our method.

In Fig. 16, instead, we report results for the rotating-wave Hamiltonian $\hat{H}_{\rm rw}$ and different cutoff frequencies and numbers of bath modes. A comparison between Figs. 15 and 16 clearly shows that the counter-rotating terms do play a crucial role

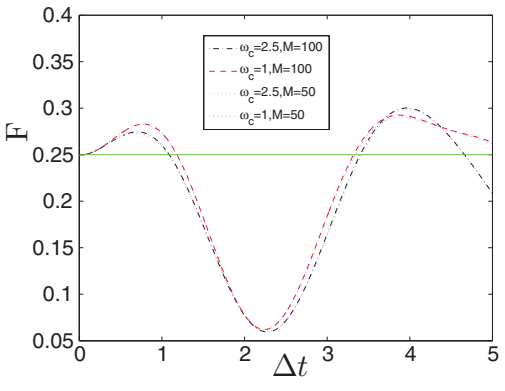

FIG. 16. (Color online) MCE results for the Choi fidelity F versus rescaled time at zero temperature for $\hat{H}_{\rm rw}$ with $\varepsilon = \Delta = 1$ and a common Ohmic bath with $\alpha = 0.09$, different cutoff frequencies, and different numbers of total bath modes. The line $F = 0.25$ is reported for reference. All the quantities plotted are dimensionless.

in this dynamics and actually effectively contribute to mediate the coherent interaction between the qubits. Also, the influence of the larger bath's cutoff frequencies at longer times is clearly represented in the plot.

Finally, notice that, as discussed in more detail in the following section, these findings about the quality of an entangling CZ gate through a bosonic bath also imply the capability for the bath to establish entanglement between the two distant qubits, which further exemplifies the potential of our method as a tool to reproduce and to study complex dynamical situations.

V. ENTANGLEMENT GENERATION

Typically, a large Choi fidelity for the (entangling) CZ gate corresponds to the generation of substantial entanglement between the two qubits. To support this statement, here, we report a brief study on the entanglement generated between two qubits. As an entanglement quantifier, we adopt the concurrence, an entanglement monotone that can be easily calculated for a system of two qubits [67]. Figures 17(a)–17(c) show the concurrence versus rescaled time for the rotating-wave Hamiltonian $\hat{H}_{\rm rw}$ with different initial states, temperatures, dynamical parameters, and numbers of modes. The degradation in quantum entanglement due to temperature is apparent [Figs. 17(a) and 17(b)] along with the speedup in the entanglement generation induced by a doubling of the modes [Fig. 17(c)].

It is also worth noticing that we did not find any region of parameters where entanglement between the two qubits was generated for the full Hamiltonian $\hat{H}$ and $M = 10$, thus, mirroring our failure in obtaining CZ fidelities larger than 0.25.

VI. CONCLUSIONS

We have presented an extensive numerical study, based on multiconfigurational Ehrenfest trajectories, on the dynamics of two qubits interacting with a common set of bosonic field modes, obtaining converged results for the Choi fidelity of an entangling CZ gate between the qubits for a rather wide range of Hamiltonian parameters and field temperatures, which cannot be covered by perturbation theory or other approximate approaches. We, thus, demonstrated the capability of tracking, analyzing in detail, and even optimizing with respect to certain ranges of some parameters, specific aspects of the coherent quantum dynamics of the qubits.

More specifically, let us summarize our main findings:

(1) We have demonstrated the ability of our method to faithfully reproduce analytical results for up to ten modes coupled through a rotating-wave Hamiltonian.

(2) We have determined optimal coupling strengths to maximize the Choi fidelity of the CZ gate between the two distant qubits.

(3) We have obtained converged results (see Appendix C for detailed information on the convergence of our numerics) for the Choi fidelity of the gate coupled by a rotating-wave Hamiltonian with the addition of local tunneling terms.

(4) We have obtained converged results, although for shorter times and weaker coupling strengths, for the Choi fidelity of the gate coupled by a spin-boson Hamiltonian.

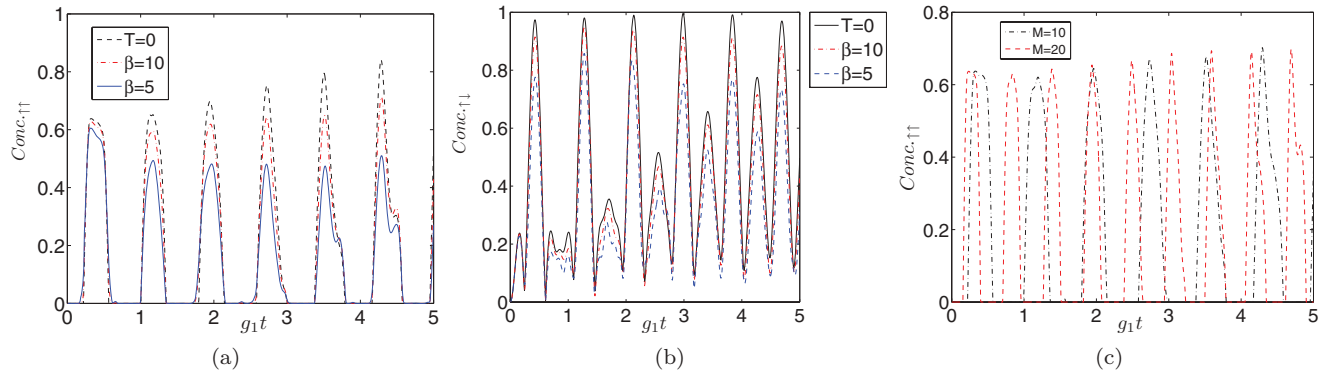

FIG. 17. (Color online) MCE results for the concurrence versus rescaled time at different temperatures for $\hat{H}_{\rm rw}$ with $g_1 = 1$ and $g_2 = 2.1$. In (a), $\varepsilon = \Delta = 0$, $M = 10$ (with $\omega_m = 0.1m$ for $1 \leqslant m \leqslant 10$), and the initial state is $|4\rangle = |\uparrow\uparrow\rangle$; in (b), $\varepsilon = \Delta = 0$, $M = 10$ (with $\omega_m = 0.1m$ for $1 \leqslant m \leqslant 10$), and the initial state is $|2\rangle = |\uparrow\downarrow\rangle$; in (c), $\varepsilon = \Delta = 1$, the initial state is $|2\rangle = |\uparrow\uparrow\rangle$, and $M = 10$ (with $\omega_m = 0.1m$ for $1 \leqslant m \leqslant 10$) for the dashed-dotted line and $M = 20$ [with $\omega_m = 0.1m$ for $1 \leqslant m \leqslant 10$ and $\omega_m = 0.1(m-10)$ for $11 \leqslant m \leqslant 20$] for the dashed line, respectively. All the quantities plotted are dimensionless.

(5) We have included the effect of finite temperatures (up to 0.2 coupling strengths) and have quantitatively determined how the temperature degrades the Choi fidelity.

(6) We have obtained converged results for the entanglement, in terms of concurrence, between the two qubits in all the dynamical situations considered above.

(7) We have obtained converged results for the Choi fidelity of the CZ gate when the interaction is mediated by a discretized Ohmic bath, showing that, in such a case, the inclusion of the counter-rotating terms actually improves the gate's quality.

We were, hence, able to properly take into account the effect of the finite bath's temperatures on the reduced dynamics of the qubits and to highlight some counterintuitive features related to the scaling of coherent signatures with the number of field modes (which we varied over the range of 1–100), showing that, at times, more mediating modes can actually be advantageous for the distribution of quantum coherence.

The main limitations of our approach lie in the difficulty of handling counter-rotating qubit-field coupling terms in the strong-coupling regime (i.e., when the coupling strengths are comparable to the inherent dynamical frequencies of the qubits). Even in such instances, we could, however, reach convergence by somewhat limiting the range of the coupling strengths.

Within such limitations, the MCE approach has, hence, been established as a powerful tool for the detailed study of complex quantum dynamics even with relatively limited resources (desktop computers), typically for systems where discrete sets of up to 100 field modes are involved.

ACKNOWLEDGMENTS

We thank H. Wichterich, R. Zhang, and L. H. Tong for their help during the writing of the code. S.-Y.Y. has been supported by a KC Wong Scholarship while pursuing this research. D.S. acknowledges financial support from EPSRC through Grants No. EPSRC EP/I014500/1 and No. NSF/EPSRC EP/J001481/1. A.S. thanks the Central Research Fund of the University of London for financial support. The authors acknowledge the use of the UCL Legion High Performance Computing Facility and associated services in the completion of this work.

APPENDIX A: EHRENFEST DYNAMICS OF THE COHERENT STATES

Here, we elaborate on Eq. (6) and explicitly derive the equation of motion for each complex parameter $\alpha_j^{(m)}$. The approximated Lagrangian $\mathcal{L}_j$ reads

$$\mathcal{L}_j = \sum_{l,n=1}^{d} c_{l,j}^* c_{n,j} \langle \boldsymbol{\alpha}_j, l | \hat{H} | \boldsymbol{\alpha}_j, n \rangle - i \sum_{l=1}^{d} c_{l,j}^* \dot{c}_{l,j} - i \sum_{l=1}^{d} |c_{l,j}|^2 \left(\frac{\dot{\boldsymbol{\alpha}}_j \cdot \boldsymbol{\alpha}_j^*}{2} - \frac{\dot{\boldsymbol{\alpha}}_j^* \cdot \boldsymbol{\alpha}_j}{2} \right), \tag{A1}$$

where $|l, \boldsymbol{\alpha}_j\rangle = |l\rangle \otimes |\boldsymbol{\alpha}_j\rangle$. Note that $\langle \boldsymbol{\alpha}_j, l | \hat{H} | \boldsymbol{\alpha}_j, n \rangle$ is just a function of the vector $\boldsymbol{\alpha}_j$ and the integers l and n, promptly evaluated by normal ordering $\hat{H}$.

The Euler-Lagrange equation for $\alpha_j^{(m)}$ then is as follows:

$$\frac{\partial \mathcal{L}_j}{\partial \alpha_j^{(m)}} = \sum_{l,n=1}^{4} c_{l,j}^* c_{n,j} \frac{\partial}{\partial \alpha_j^{(m)}} \langle \boldsymbol{\alpha}_j, l | \hat{H} | \boldsymbol{\alpha}_j, n \rangle + i \sum_{l=1}^{d} |c_{l,j}|^2 \frac{\dot{\alpha}_j^{(m)*}}{2} = -i \frac{d}{dt} \left(\sum_{l=1}^{d} |c_{l,j}|^2 \frac{\alpha_j^{(m)*}}{2} \right) = \frac{d}{dt} \frac{\partial \mathcal{L}_j}{\partial \dot{\alpha}_j^{(m)}}, \tag{A2}$$

which, by neglecting the time dependence of $c_{l,j}$ [setting $\frac{d}{dt}(\sum_{l=1}^{d} |c_{l,j}|^2) = 0$], can be rearranged to obtain

$$\dot{\alpha}_j^{(m)*} = i \frac{\sum_{l,n=1}^{4} c_{l,j}^* c_{n,j} \frac{\partial}{\partial \alpha_j^{(m)}} \langle \boldsymbol{\alpha}_j, l | \hat{H} | \boldsymbol{\alpha}_j, n \rangle}{\sum_{l=1}^{d} |c_{l,j}|^2}. \tag{A3}$$

This equation governs the evolution of the vectors $\boldsymbol{\alpha}_j$ in our numerics.

APPENDIX B: DYNAMICS OF THE STATE VECTOR

For the sake of completeness, let us also report the system of dynamical equations (Schrödinger equation on the subspace

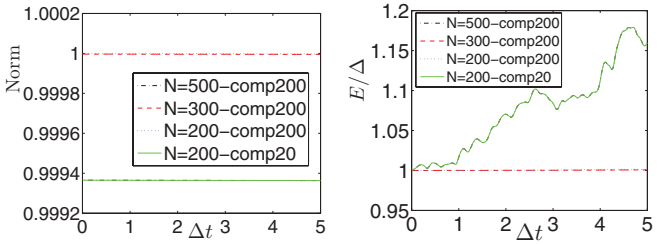

FIG. 18. (Color online) (a) Norm and (b) E/Δ (where E is the expectation value of energy) for MCE results at zero temperature for $\hat{H}_{\rm rw}$ with $\varepsilon = \Delta = g_1 = 1$, $g_2 = 2.7$, $M = 10$ (with $\omega_m = 0.1m$ for $1 \leqslant m \leqslant 10$), and different values of N and comp. All the quantities plotted are dimensionless.

spanned by the basis grid) for the parameters $c_{l,j}$, which can be derived by Eq. (2) and reads

$$\sum_{k=1}^{N}\left[i\Omega_{jk}\dot{c}_{l,k} + i\Omega_{jk}\left(\boldsymbol{\alpha}_j^*\cdot\dot{\boldsymbol{\alpha}}_k - \frac{\boldsymbol{\alpha}_j^*\cdot\dot{\boldsymbol{\alpha}}_j}{2} - \frac{\dot{\boldsymbol{\alpha}}_j^*\cdot\boldsymbol{\alpha}_j}{2}\right)c_{l,k} - \sum_{h=1}^{d}\langle\boldsymbol{\alpha}_j,l|\hat{H}|h,\boldsymbol{\alpha}_k\rangle c_{h,k}\right] = 0,$$

where $\Omega_{jk} = \langle\boldsymbol{\alpha}_j|\boldsymbol{\alpha}_k\rangle$. To enhance the stability of the numerical treatment, the parameters $c_{l,j}$ are actually redefined by multiplication with a smooth phase factor (essentially, a semiclassical action).

APPENDIX C: CONVERGENCE OF MCE RESULTS

To give an idea of the quality and range of reliability of our results, here, we provide some evidence of the convergence of our numerics.

Throughout our paper, the centers of the initial set of coherent states are distributed in phase space with a Gaussian distribution with standard deviation $1/\text{comp}$. The parameter comp is a free parameter of the paper, which is tuned to optimize convergence. As indicators of the quality of the numerics, we will observe the convergence of specific entries of the density matrix of the two qubits ϱ as well as the norm $\text{Tr}(\varrho)$ and the expectation value of the energy $\text{Tr}(\hat{H}\varrho)$, which are obviously conserved in the exact dynamics. Notice that

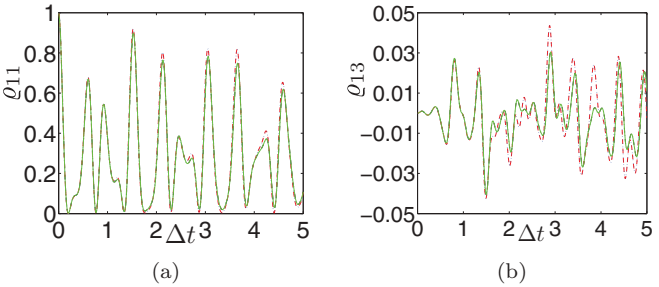

FIG. 19. (Color online) Entries of the qubits' density matrix (a) ϱ_{11} and (b) ϱ_{13} for MCE results at zero temperature for $\hat{H}_{\rm rw}$ with $\varepsilon = \Delta = g_1 = 1$, $g_2 = 2.7$, $M = 10$ (with $\omega_m = 0.1m$ for $1 \leqslant m \leqslant 10$), and different values of N and comp. The line label is the same as in Figs. 18(a) and 18(b). All the quantities plotted are dimensionless.

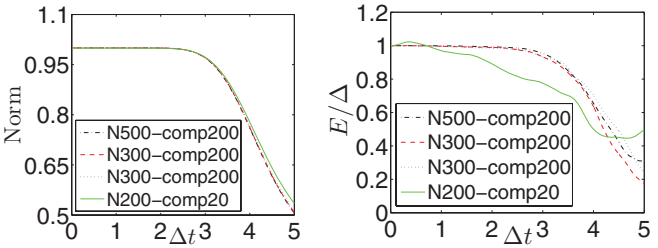

FIG. 20. (Color online) (a) Norm and (b) E/Δ (where E is the expectation value of energy) for MCE results at zero temperature for $\hat{H}$ with $\varepsilon = \Delta = g_1 = g_2 = 1$, $M = 10$ (with $\omega_m = 0.1m$ for $1 \leqslant m \leqslant 10$), and different values of N and comp. All the quantities plotted are dimensionless.

our method does not have any built-in routine guaranteeing the conservation of the state vector's norm so that $\text{Tr}(\varrho)$ is a relevant figure of merit to assess its reliability.

Figures 18(a) and 18(b) display the norm and expectation value of the energy for a case of non-number-conserving rotating-wave Hamiltonian (initial spin state $|\uparrow\uparrow\rangle$), whereas, in Figs. 19(a) and 19(b), the entries ϱ_{11} and ϱ_{13} are plotted. The reliability of the numerics over the whole time frame considered is apparent (for the large enough compression parameter comp) in terms of both convergence with increasing number N of coherent states and of conservation of invariant quantities. As anticipated, the situation is much more dire for the full Hamiltonian $\hat{H}$. In this case, Figs. 20 and 21 show that our numerics are only reliable up to rescaled times around 2.5, after which, both convergence and norm and energy conservation are lost, even at smaller coupling strengths (in that $g_2 = 1$ rather than $g_2 = 2.7$ as before). By reducing both couplings g_1 and g_2 to 0.5, the convergence can be extended to slightly more than $t = 5$ as is the case in the plots reported in our paper.

It is important to stress that the inconsistencies shown in Figs. 20 and 21 are only reported to illustrate the regime of validity of our method. *All data corresponding to times where any check, based on matrix elements' convergence, norm conservation, or energy conservation failed, have been discarded in the present paper and bore no consequence whatsoever on our analysis.*

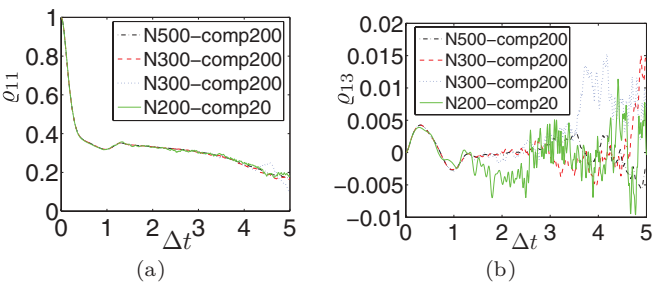

FIG. 21. (Color online) Entries of the qubits' density matrix (a) ϱ_{11} and (b) ϱ_{13} for MCE results at zero temperature for $\hat{H}$ with $\varepsilon = \Delta = g_1 = g_2 = 1$, $M = 10$ (with $\omega_m = 0.1m$ for $1 \leqslant m \leqslant 10$), and different values of N and comp. All the quantities plotted are dimensionless.

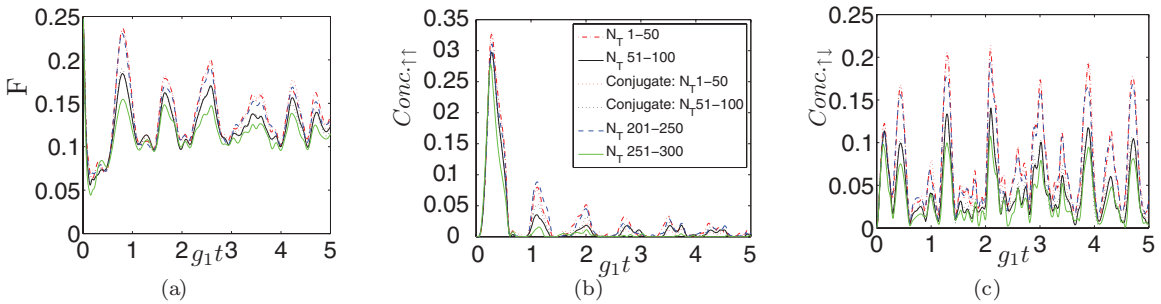

FIG. 22. (Color online) (a) Choi fidelity, concurrence for two different separable initial states (b) $|\uparrow\uparrow\rangle$, and (c) $|\uparrow\downarrow\rangle$ versus rescaled time for $\hat{H}_{\rm rw}$ with $\varepsilon = \Delta = 0$, $g_1 = 1$, $g_2 = 2.1$, $\beta = 0.5$, and different values of N_T and M. In all plots, $M = 10$ with $\omega_m = 0.1m$ for $1 \leqslant m \leqslant 10$. "Conjugate" refers to the fact that, for those curves, the initial centers of the coherent states $\boldsymbol{\alpha}_j$ are in complex-conjugate pairs.

Finally, we show three examples of convergence of our results at finite temperatures (here, $\beta = 0.5$) with respect to the increase in the number of states N_T over which, the thermal distribution of Eq. (16) is sampled [Figs. 22(a)–22(c)].

[1] J. I. Cirac and P. Zoller, Phys. Rev. Lett. **74**, 4091 (1995).
[2] J. I. Cirac, P. Zoller, H. J. Kimble, and H. Mabuchi, Phys. Rev. Lett. **78**, 3221 (1997).
[3] S. J. van Enk, H. J. Kimble, J. I. Cirac, and P. Zoller, Phys. Rev. A **59**, 2659 (1999).
[4] T. Pellizzari, Phys. Rev. Lett. **79**, 5242 (1997).
[5] M. B. Plenio, S. F. Huelga, A. Beige, and P. L. Knight, Phys. Rev. A **59**, 2468 (1999).
[6] A. Rauschenbeutel, G. Nogues, S. Osnaghi, P. Bertet, M. Brune, J. M. Raimond, and S. Haroche, Phys. Rev. Lett. **83**, 5166 (1999).
[7] S. B. Zheng and G. C. Guo, Phys. Rev. Lett. **85**, 2392 (2000).
[8] J. Pachos and H. Walther, Phys. Rev. Lett. **89**, 187903 (2002).
[9] D. Leibfried, B. De Marco, V. Meyer, D. Lucas, M. Barrett, J. Britton, W. M. Itano, B. Jelekovic, C. Langer, T. Roseband, and D. J. Wineland, Nature (London) **422**, 412 (2003).
[10] S. Clark, A. Peng, M. Gu, and S. Parkins, Phys. Rev. Lett. **91**, 177901 (2003).
[11] S. B. Zheng, Phys. Rev. A **70**, 052320 (2004).
[12] Y. F. Xiao, X. M. Lin, J. Gao, Y. Yang, Z. F. Han, and G. C. Guo, Phys. Rev. A **70**, 042314 (2004).
[13] M. Paternostro, G. Falci, M. Kim, and G. M. Palma, Phys. Rev. B **69**, 214502 (2004).
[14] S. D. Barrett and P. Kok, Phys. Rev. A **71**, 060310(R) (2005); S. C. Benjamin, *ibid.* **72**, 056302 (2005).
[15] X. B. Zou and W. Mathis, Phys. Rev. A **71**, 042334 (2005).
[16] X. F. Zhou, Y. S. Zhang, and G. C. Guo, Phys. Rev. A **71**, 064302 (2005).
[17] Y. L. Lim, S. D. Barrett, A. Beige, P. Kok, and L. C. Kwek, Phys. Rev. A **73**, 012304 (2006).
[18] A. Serafini, S. Mancini, and S. Bose, Phys. Rev. Lett. **96**, 010503 (2006).
[19] T. P. Spiller, K. Nemoto, S. L. Braunstein, W. J. Munro, P. van Loock, and G. J. Milburn, New J. Phys. **8**, 20 (2006).
[20] Z. Q. Yin and F. L. Li, Phys. Rev. A **75**, 012324 (2007).
[21] S. Y. Ye, Z. R. Zhong, and S. B. Zheng, Phys. Rev. A **77**, 014303 (2008); S. Y. Ye and S. B. Zheng, Opt. Commun. **281**, 1306 (2008).
[22] X. B. Zou, Y. F. Xiao, S. B. Li, Y. Yang, and G. C. Guo, Phys. Rev. A **75**, 064301 (2007).
[23] X. Y. Lü, J. B. Liu, C. L. Ding, and J. H. Li, Phys. Rev. A **78**, 032305 (2008).
[24] J. Busch, E. S. Kyoseva, M. Trupke, and A. Beige, Phys. Rev. A **78**, 040301(R) (2008).
[25] H. J. Kimble, Nature (London) **453**, 1023 (2008).
[26] J. Li, K. Chalapat, and G. S. Paraoanu, Phys. Rev. B **78**, 064503 (2008).
[27] S. B. Zheng and G. C. Guo, Phys. Rev. A **73**, 052328 (2006); S. B. Zheng, Appl. Phys. Lett. **94**, 154101 (2009).
[28] Z. B. Yang, H. Z. Wu, W. J. Su, and S. B. Zheng, Phys. Rev. A **80**, 012305 (2009).
[29] Z. B. Yang, S. Y. Ye, A. Serafini, and S. B. Zheng, J. Phys. B **43**, 085506 (2010).
[30] S. Y. Ye, Z. B. Yang, S. B. Zheng, and A. Serafini, Phys. Rev. A **82**, 012307 (2010).
[31] P. Pei, F. Y. Zhang, C. Li, and H. S. Song, Phys. Rev. A **84**, 042339 (2011).
[32] W. L. Yang, Z. Q. Yin, Z. Y. Xu, M. Feng, and C. H. Oh, Phys. Rev. A **84**, 043849 (2011).
[33] M. Alexanian, Phys. Rev. A **84**, 052302 (2011).
[34] M. H. Beck, A. Jackle, G. A. Worth, and H.-D. Mayer, Phys. Rep. **324**, 1 (2000).
[35] H. Wang, J. Chem. Phys. **103**, 9948 (2000).
[36] H. Wang and M. Thoss, New J. Phys. **10**, 115005 (2008).
[37] I. Burghardt, H.-D. Mayer, and L. S. Cederbaum, J. Chem. Phys. **111**, 2927 (1999).
[38] N. Makri, J. Phys. Chem. **102**, 4414 (1998).
[39] F. Nesi, E. Paladino, M. Thorwart, and M. Grifoni, Phys. Rev. B **76**, 155323 (2007).
[40] J. Prior, A. W. Chin, S. F. Huelga, and M. B. Plenio, Phys. Rev. Lett. **105**, 050404 (2010).
[41] D. V. Shalashilin, J. Chem. Phys. **130**, 244101 (2009).
[42] D. V. Shalashilin, J. Chem. Phys. **132**, 244111 (2010).
[43] D. V. Shalashilin and M. S. Child, J. Chem. Phys. **113**, 10028 (2000); **114**, 9296 (2001); **115**, 5367 (2001); **128**, 054102 (2008).
[44] This duality is usually referred to as the "Choi-Jamiolkowski" isomorphism in the quantum-information literature. For an

interesting disambiguation between Choi and Jamiolkowski isomorphism and much else, see M. S. Leifer and R. W. Spekkens, arXiv:1107.5849v2.
[45] M. D. Choi, Linear Algebr. Appl. **10**, 285 (1975).
[46] V. P. Belavkin and P. Staszewski, Rep. Math. Phys. **24**, 49 (1986).
[47] J. D. Joannopoulos, S. G. Johnson, J. N. Winn, and R. D. Meade, *Photonic Crystals: Molding the Flow of Light* (Princeton University Press, New York, 2008).
[48] P. Lodahl, A. F. van Driel, I. S. Nikolaev, A. Irman, K. Overgaag, D. Vanmaekelbergh, and W. L. Vos, Nature (London) **430**, 654 (2004).
[49] D. Porras, F. Marquardt, J. von Delft, and J. I. Cirac, Phys. Rev. A **78**, 010101(R) (2008); D. Porras, P. A. Ivanov, and F. Schmidt-Kaler, Phys. Rev. Lett. **108**, 235701 (2012).
[50] S.-Y. Ye, D. Shalashilin, and A. Serafini (unpublished).
[51] M. J. Bremner, C. M. Dawson, J. L. Dodd, A. Gilchrist, A. W. Harrow, D. Mortimer, M. A. Nielsen, and T. J. Osborne, Phys. Rev. Lett. **89**, 247902 (2002).
[52] D. Braun, Phys. Rev. Lett. **89**, 277901 (2002).
[53] M. B. Plenio and S. F. Huelga, Phys. Rev. Lett. **88**, 197901 (2002).
[54] M. S. Kim, J. Lee, D. Ahn, and P. L. Knight, Phys. Rev. A **65**, 040101 (2002).
[55] T. S. Cubitt, F. Verstraete, W. Dur, and J. I. Cirac, Phys. Rev. Lett. **91**, 037902 (2003).
[56] F. Benatti, R. Floreanini, and M. Piani, Phys. Rev. Lett. **91**, 070402 (2003).
[57] T. Vorrath and T. Brandes, Phys. Rev. B **68**, 035309 (2003).
[58] F. Benatti and R. Floreanini, J. Opt. B **7**, S429 (2005).
[59] S. Oh and J. Kim, Phys. Rev. A **73**, 062306 (2006).
[60] D. Solenov, D. Tolkunov, and V. Privman, Phys. Lett. A **359**, 81 (2006).
[61] D. Solenov, D. Tolkunov, and V. Privman, Phys. Rev. B **75**, 035134 (2007).
[62] J. H. An, S. J. Wong, and H. G. Luo, Physica A **382**, 753 (2007).
[63] T. Choi and H. J. Lee, Phys. Rev. A **76**, 012308 (2007).
[64] L. D. Contreras-Pulido and R. Aguado, Phys. Rev. B **77**, 155420 (2008).
[65] D. P. S. McCutcheon, A. Nazir, S. Bose, and A. J. Fisher, Phys. Rev. A **80**, 022337 (2009).
[66] F. Benatti, R. Floreanini, and U. Marzolino, Europhys. Lett. **88**, 20011 (2009).
[67] W. K. Wootters, Phys. Rev. Lett. **80**, 2245 (1998).